Micropositioning mechatronics system based on FPGA architecture

Ervin Kamenar and Saša Zelenika
University of Rijeka, Faculty of Engineering and Centre for Micro and Nano Sciences and Technologies, Rijeka, Croatia
ekamenar@riteh.hr, sasa.zelenika@riteh.hr

Abstract – In this paper a micropositioning mechatronics system is conceived and described. Its mechanical design is optimized in order to achieve high precision displacements. High speed closed-loop feedback control is obtained by using both PID and ramp control algorithms programmed as virtual instruments (VI) on an FPGA (Field Programmable Gate Array) module. User controls are programmed in an independent Host VI. A Linear Variable Differential Transformer (LVDT) is employed as a position feedback sensor, while positioning accuracy and repeatability are experimentally assessed by using a Michelson-type laser Doppler interferometric system. Different experiments with point-to-point positioning are conducted. In the first set of experiments, positioning with 100 µm steps is performed. In a second step, 10 mm positioning experiments are done. The system shows a marked nonlinearity when longer positioning steps are used; this nonlinearity influences significantly the output error. It is hence found that the main contribution to system's nonlinearity is caused by the LVDT. The error is compensated via system linearization by an experimentally obtained analytical function which is programmed in the LabVIEW Host VI. Positioning accuracy and repeatability are finally assessed experimentally again and true micrometric positioning is achieved.

I. INTRODUCTION

High-precision positioning over stroke lengths from several tens of millimetres up to several metres is often needed in manufacturing systems where this aim is frequently achieved by using positioning mechanisms driven by rotary motors [1]. In this frame, an accurate tracking performance coupled with specified requirements for positioning accuracy and repeatability is essential in realizing ultra-precision devices. Moreover, nowadays there is a clear tendency towards reducing the dimensions of the products, i.e. towards miniaturization [2]. In dealing with these challenges, improving the mechanical elements that make up the considered system is generally rather expensive [1-3]. On the other hand, reliable control systems offer a good alternative [2-5].

Field Programmable Gate Arrays (FPGA [6]) represent a possible technological approach in the implementation of suitable control typologies. FPGA technology has been recently widely used in many commercial, as well as in industrial applications. FPGAs are characterized by flexibility, high performance and low-level reconfigurability. Also, a very important differentiating feature with respect to conventional Central Processor Units (CPUs) is that a single CPU can process only a single instruction per time cycle. On the other hand, an FPGA can be configured as several virtual processors capable of functioning in parallel. Moreover, FPGAs allow digital solutions for the controllers used in closed-loop systems. In fact, an important prerequisite for good control is a feedback-based closed-loop control system. A good feedback implies, in turn, the usage of sensors with high resolution and minimal nonlinearity [7-9].

In this work, a micropositioning mechatronics system is conceived. Digital high speed closed-loop feedback control is implemented. Two types of control algorithms are used: a digital proportional-integral-derivative (PID) controller and a ramp control algorithm. The PID controller is custom designed since the available LabVIEW software does not include the LabVIEW PID Control Toolkit license. On the other hand, the ramp

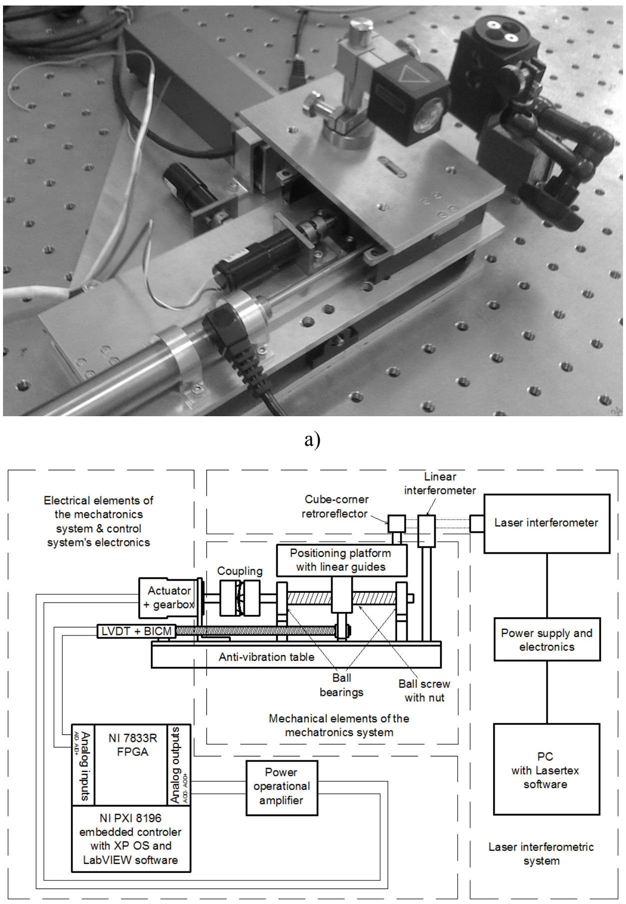

a)

b)

Figure 1. Experimental set-up (a) and its scheme (b)

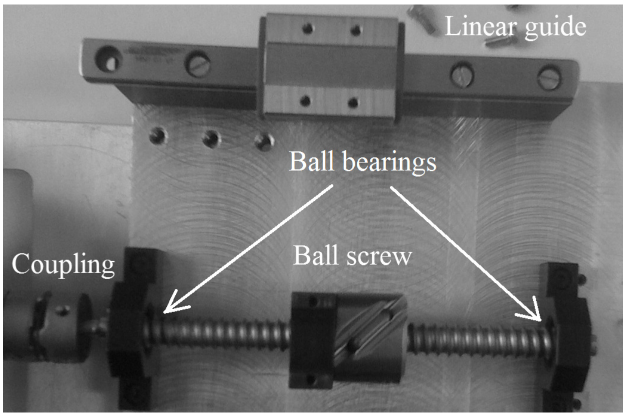

Figure 2. Main mechanical parts of the system

controller is based on a linearly decreasing actuator input voltage proportional to the distance of the moving part to the defined reference position.

II. EXPERIMENTAL SET-UP

The development and assessment of the performances of the conceived micropositioning mechatronics system is performed on a suitable experimental set-up depicted in Figure 1. The single axis high precision system is constituted by a DC actuator, a feedback sensor, mechanical elements, the control system and the laser interferometric system used for the nanometric assessment of the positioning accuracy and repeatability.

A. Actuator and Feedback Sensor

The mechatronics system is driven by a Faulhaber M 1724 006 SR DC actuator with a nominal voltage U_N = 6 V, a no load speed n_0 = 8600 rpm and dimensions ϕ = 17 x L = 24 mm. The motor is integrated with a two-stage L_g = 17.7 mm Faulhaber series 15A plastic planetary gearhead having a reduction ratio i = 19:1 [10].

The used feedback sensor is an Omega series LD610-50 Linear Variable Differential Transformer (LVDT) with a measurement range of l = ± 50 mm (100 mm). An LVDT is a linear displacement/position sensor which consists of a static and a moving element. The static element bears a central primary winding excited with an AC excitation voltage V_e = 2 V RMS, which is located between two symmetrical secondary windings. The moving element consists of a separated cylindrical core made of a Ni-Fe alloy, mechanically connected to the moving part of the system. When the system moves, a sinusoidal voltage with an amplitude proportional to the movement is generated on the secondary windings [11]. AC voltage is conditioned by the Boxed Inline Conditioning Module (BICM [12]) which is embedded with the LVDT and its output is set to cover the full scale of the induced voltage $V_{BICM\,\max}$ = ± 10 Vdc. The BICM module also generates the AC excitation voltage of the primary winding.

B. Mechanical Elements of the Mechatronics System

Although, in general, various types of sliding and rolling leadscrews are used in high precision applications, ball screws are the most common solution in practical applications [13]. In the developed experimental set-up, the rotation of the DC motor is therefore converted to linear displacement by using an SKF type SH miniature ball screw with integrated tube recirculation having a nominal diameter d_0 = 6 mm, a p = 2 mm lead, a nominal maximum backlash B = 50 μm and a practical efficiency of η_p = 94% [14]. The screw is supported by employing Miniature SKF 618/4 d = 4 mm, D = 9 mm, b = 2.5 mm ball bearings [15]. The motor is connected to the ball screw by using a miniature aluminium Misumi MCGS13-3-3 coupling with a compliant polyimide disc enabling the compensation of lateral and angular misalignments and having a nominal outer diameter D_C = 16 mm, inner diameters $d_1 = d_2$ = 3 mm and the length l_C = 13 mm [16].

Schneeberger MINIRAIL profiled miniature guideways MN 7 with fixed part dimensions: $l_f/w_f/h_f$ = 85 /7/4.5 mm and moving part dimensions: $l_m/w_m/h_m$ = 24.6/ 17/6.5 mm are used as linear guides allowing the sliding of the movable part of the system [17].

The described ball screw, ball bearings and linear guideways are shown in Figure 2.

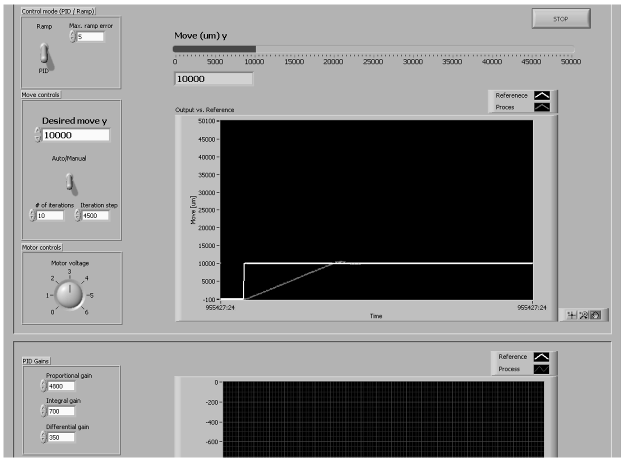
Figure 3. Host VI front panel

C. Control System

The control system of the conceived mechatronics device consists of a National Instruments (NI) PXI-1050 chassis, including a PXI-8196 embedded controller and a reconfigurable PXI-7833R FPGA module.

The NI PXI-1050 chassis has eight PXI (PCI eXtensions for Instrumentation) slots with four integrated Signal Conditioning Extension for Instrumentation (SCXI) subsystem slots. The SCXI system is connected via a bus to the PXI slots enabling the control of the

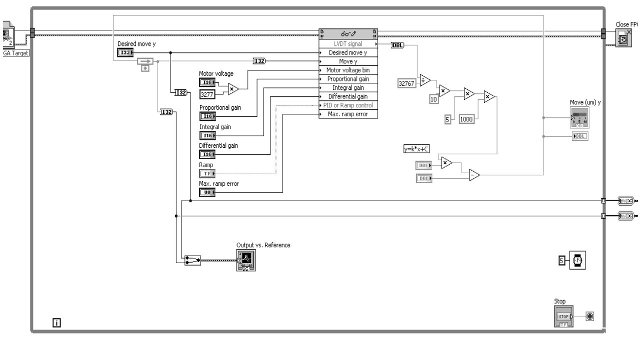
Figure 4. Host VI block diagram

SCXI system in a multiplex mode [18]. The NI PXI-8196 embedded controller is a modular PC in a PXI running on Windows XP OS [19].

The NI PXI-7833R FPGA module with a Virtex-II 3M gate FPGA chip is equipped with a reconfigurable input/output (RIO) hardware which allows processing of data on the card. It has eight analog 16-bit inputs, eight analog 16-bit outputs and 96 digital lines configurable as inputs, outputs, counters, or custom logic at rates of up to 40 MHz. Analog inputs and outputs have a full scale range of $V_{AO/I} = \pm\ 10$ V [20]. The analog input 0 (AI0) of the FPGA module is used to connect the LVDT position feedback sensor of the developed mechatronics system. The obtainable theoretical resolution r of the LVDT can thus be calculated as:

$$r = \frac{l}{2^{16}} = \frac{100\,mm}{65535} \approx 1.5\,\mu m \qquad (1)$$

where l is the measurement range of the used LVDT.

On the other hand, the analog output AO0 is used to drive the DC actuator. Since each analog output of the NI PXI-7833R module can deliver a maximum output current of 25 mA, it cannot directly power the DC actuator which has a no-load current I_0 = 20 mA and a stall current of approximately I_H = 400 mA. An inverting Texas Instruments LM675 power operational amplifier with a maximum output current $I_{\max}$ = 3 A and a voltage gain set to A = 1 is thus used [21]. The value of the voltage gain is set to one since the maximum actuator voltage is 6 V and the output of the FPGA module has a full scale range of 10 V. Only current amplifying is thus needed in order to drive the selected DC actuator.

The control algorithms are programmed in the LabVIEW program environment [22]. The latter consists of two main virtual instruments (VI [23]): the Host VI and the FPGA VI. The Host VI is executed on the host computer (the PXI-8196 embedded controller) and includes user controls and indicators. The FPGA VI is designed and compiled on the host PC and exported to the FPGA module. Each VI has its front panel that consists of user controls and indicators, and its block diagram, which consists of the coded parts of the VI. The Host VI front panel is shown in Figure 3 while its block diagram is given in Figure 4.

The FPGA VI is used to implement the control algorithms, i.e., in the herein considered case, the PID and the ramp control algorithms described in section III.

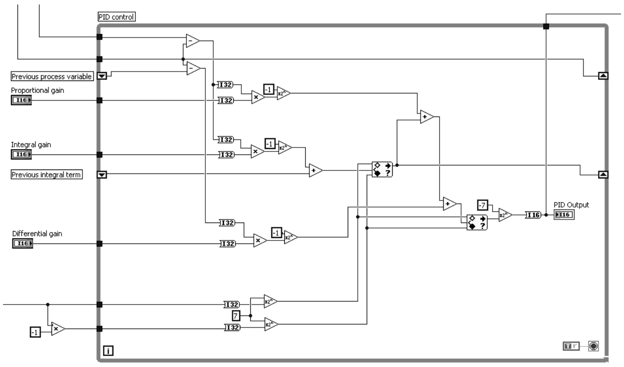

Figure 5. PID control FPGA VI block diagram

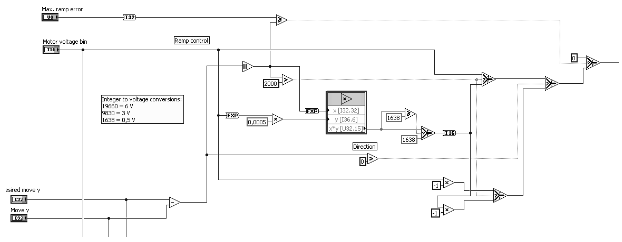

Figure 6. Ramp control FPGA VI block diagram

In Figure 5 the PID version of the FPGA block diagram is depicted, while in Figure 6 the ramp algorithm, implemented as the FPGA block diagram, is shown.

The independence of the host computer (where the Host VI is running) and the FPGA VI is one of the main advantages of systems based on FPGA architecture. In fact, if the host computer stops to operate, the user will not be able to read the indicator values or interactively control the system, but the FPGA VI will still be running and executing its program.

D. *Laser Interferometric System*

In this work the mobile Lasertex LSP 30-3D [24] Michelson-type laser Doppler interferometric system is used to assess the positioning accuracy and repeatability achieved by the used mechatronics system. This is a two-frequency laser interferometer which can be used in optical set-ups for linear and angular positioning or velocity measurements, as well as for straightness, flatness or squareness measurements. The available sensors allow compensating in real-time the environmental influences due to pressure, temperature and humidity variations during the measurements. Mounting and alignment errors such as the dead path, cosine and Abbe errors [25] have been minimized by performing a careful iterative mounting procedure.

To perform the needed nanometric measurements, a linear optical set-up is used. As shown in Figure 7, it is made of a laser head with an integrated receiver, the linear interferometer (reference cube-corner) and the linear cube-corner retroreflector. In the specific application, the laser head and the interferometer are mounted on the static base, while the retroreflector is mounted on the moving part (see Figure 1a).

III. CONTROL METHODS

High speed closed-loop feedback control is obtained by using a PID and a ramp control algorithm.

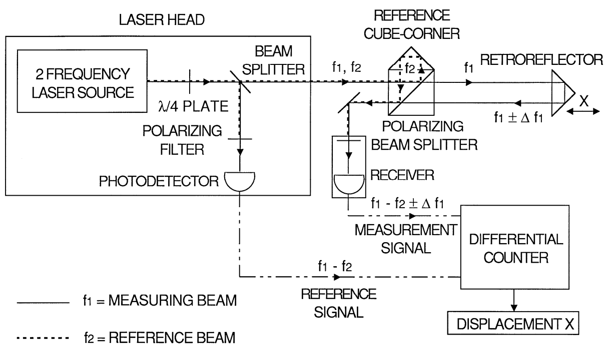

Figure 7. Michelson-type laser Doppler interferometric system

A. PID Controller

PID controllers have been widely used for many years in various industrial applications and control systems; in fact, PID is the most commonly used feedback controller. It is a closed-loop feedback control typology based on three terms – proportional (K_P), integral (K_I) and derivative (K_D). These parameters, known as PID gains, multiply in the feedback loop the error determined by the feedback sensor of the considered system and have different numeric values depending on the system architecture and its operating conditions [26].

The error value $e(t)$, represented by the difference between the set reference position (set point) $y_0(t)$ and the reached position (process value – PV) $y(t)$, measured via the feedback sensor, can be expressed as:

$$e(t) = y_0(t) - y(t) \tag{2}$$

In the time domain, the output of the PID control algorithm $u(t)$, can then be defined as [26]:

$$u(t) = K_P \cdot \left(e(t) + \frac{1}{T_I} \cdot \int_0^t e(\tau) \cdot d\tau + T_D \frac{d\, e(t)}{dt} \right) \tag{3}$$

where T_I is the integral time constant, T_D is the derivative time constant and τ is the integrating variable that can vary in the time interval from 0 to the actual time t.

To get the discrete form of the controller, the integral and the derivative terms are approximated as [27]:

$$\int_0^t e(\tau) \cdot d\tau \approx T \cdot \sum_{k=0}^{n} e(k)$$

$$\frac{d\, e(t)}{dt} \approx \frac{e(n) - e(n-1)}{T} \tag{4}$$

$$t = n \cdot T$$

where $e(n)$ is the discrete proportional and derivative error term, $e(k)$ is the integral error term, t is time, k is the summation variable for the discrete integral term, n is the discrete time step, and T is the signal sampling period.

The integral and derivative PID gains can hence be calculated from the integral and derivate time constant as [27]:

$$K_I = \frac{K_P \cdot T}{T_I}, \quad K_D = \frac{K_P \cdot T_D}{T} \tag{5}$$

Equations (3-5) make it possible to express the discrete PID controller as [27]:

$$u(n) = K_P \cdot e(n) + K_I \sum_{k=0}^{n} e(k) + K_D [e(n) - e(n-1)] \tag{6}$$

where $u(n)$ is the output from the discrete controller.

To avoid that a change in the defined set point (in this case the reference position) induces unwanted rapid changes (i.e. sharp spikes or derivative kicks) in the control signal, the controller is improved by multiplying the process value (defined as the reached position in two consecutive time steps – i.e. not the error term) by the derivative gain. These rapid changes could otherwise create serious problems for electronic circuitry [28]. Finally, the discrete PID algorithm, which can be implemented on the FPGA module, can be expressed as [28]:

$$u(n) = K_P e(n) + K_I \sum_{k=0}^{n} e(k) + K_D [y(n) - y(n-1)] \tag{7}$$

where $y(n)$ and $y(n\text{–}1)$ are the reached positions measured via the feedback sensor in two subsequent discrete time steps. The block diagram of the digital PID controller implemented on the FPGA module is shown in Figure 5.

It is worth noting here that various methods are commonly used for tuning the PID gains, some of them being the Ziegler Nichols, the Cohen-Coon or the Tyreus-Luyben tuning method [29]. In this work the tuning of the PID controller parameters is conducted in two steps. First, the Ziegler-Nichols method is used to achieve a rough estimate of the gains; in a second step, an experimental method of fine-tuning of the PID parameters is performed.

B. Ramp Control

The ramp control algorithm is based on a linearly decreasing driving voltage proportional to the distance of the moving part to the reference position. Maximum voltage $V_{R\max}$ is therefore delivered to the actuator up to the point distant two millimetres from the reference point. The input voltage is then linearly decreased from the maximum available value to a user-defined minimal value (in the considered case, this value is $V_{R\min}$ = 0.5 V so as to enable the overcoming of mechanical nonlinearities such as sticktion). When the moving part finally reaches the reference position – within the limits of the defined maximal acceptable positioning error, the driving voltage is set to zero. The whole cycle is adapted to the operation of the used mechatronics system so as to avoid overshoots when reaching the reference position. The used ramp control function is shown in Figure 8.

IV. Experiments

To assess the performances of the described mechatronics system, whose control is based on FPGA architecture, in achieving micropositioning, a set of point-to-point experiments using both the PID and the ramp control typologies is performed.

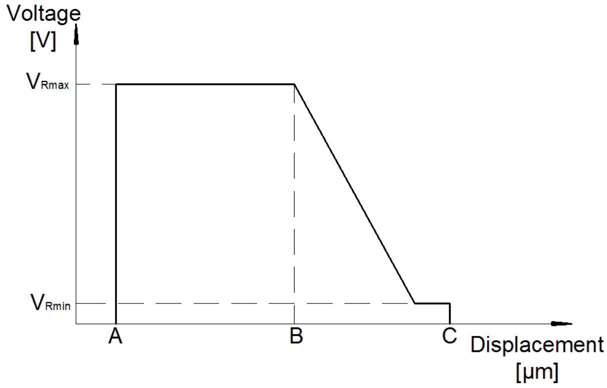

Figure 8. Ramp control function

TABLE I. MEASUREMENTS FOR 100 μm STEPS – ERRORS IN μm

	PID	*Ramp*		*PID*	*Ramp*
Point no.	***Error***	***Error***	***Point no.***	***Error***	***Error***
1	-2.8	-1.2	6	-6.2	-1.8
2	-7.6	-0.8	7	3.9	-0.8
3	-2.5	-1.9	8	-1.1	-1.1
4	-1.1	2.5	9	-6.5	0.4
5	-6.5	3.0	10	-4.6	-1.5

In a first instance, point-to-point positioning in a micrometric range of displacements, i.e. with 100 μm steps is implemented. Long range, ten millimetre steps are executed next.

A. *Hundred Micrometre Displacements*

In this set of experiments, each measurement is repeated 10 times. The mechatronics system performs in each move a displacement from the initial position to the reference position in 100 μm steps. The first set of measurements is performed by employing PID control, the second one using the described ramp control algorithm. To obtain optimal system response, the PID gains are set to the following values: $K_P = 4700$, $K_I = 600$, $K_D = 190$.

The thus obtained measurement results in terms of the errors in μm are given in Table I. It can hence be calculated that, in the case when PID control is used, positioning accuracy and repeatability are, respectively, 2.68 μm and 3.07 μm. When the ramp control algorithm is used instead, these values are 1.75 μm and 0.32 μm.

B. *Ten Millimetre Displacements*

When longer travel ranges are implemented, the system output results in a marked nonlinearity which significantly influences the resulting positioning error. In fact, from the results listed in Table II it is evident that, when PID control with the same gains as in the previous case is used, positioning accuracy and repeatability are, respectively, 44.34 μm and 3.53 μm. With ramp control, accuracy is 48.62 μm, while repeatability is 3.37 μm.

C. *Ten Millimetre Displacements with Linearization*

A careful analysis of the system architecture allowed establishing that the LVDT sensor has the main influence on the observed system's nonlinearity in the case of longer travel ranges. By using the laser interferometric system, repetitive measurements with 1 mm steps in the whole 0 – 10 mm range, coupled with an interpolating procedure implemented in the Matlab software [30], allowed determining that the linearization function to be applied to the values of displacements x measured via the LVDT has the form:

$$f(x) = 1{,}006 \cdot x + 7 \tag{8}$$

This linearization function is hence programmed in the LabVIEW Host VI and, considering that the linearization function causes a different behaviour of the system, the PID gains are slightly modified ($K_P = 4800$, $K_I = 700$, $K_D = 350$). Long travel range experiments are hence performed again and the obtained results are given in Table III. It is clear that a marked improvement is obtained and a positioning accuracy of 1.18 μm with a repeatability of 1.86 μm can be calculated. In the case of ramp control, positioning accuracy and repeatability are, respectively, 0.73 μm and 2.34 μm.

TABLE II. MEASUREMENTS FOR 10 mm STEPS W/O LINEARIZATION – ERRORS IN μm

	PID	*Ramp*		*PID*	*Ramp*
Point no.	***Error***	***Error***	***Point no.***	***Error***	***Error***
1	37.3	47.4	6	49.4	55.5
2	48.8	50.3	7	46.4	52.7
3	44.5	49.8	8	42.5	48.5
4	40.3	46.6	9	45.1	44.1
5	42.9	46.7	10	46.2	44.6

TABLE III. MEASUREMENTS FOR 10 mm STEPS WITH LINEARIZATION – ERRORS IN μm

	PID	*Ramp*		*PID*	*Ramp*
Point no.	***Error***	***Error***	***Point no.***	***Error***	***Error***
1	1.1	0.6	6	3.6	3.6
2	0.7	2.4	7	3.2	-0.5
3	2.6	-2.7	8	2.2	0.2
4	-0.6	-2.6	9	-1.7	-1.2
5	2.4	-3.6	10	-1.7	-3.5

V. CONCLUSIONS AND OUTLOOK

In this work a single-axis micropositioning mechatronics system is developed. Its mechanical design is optimized in order to achieve high precision positioning. High speed closed-loop feedback control is obtained by using PID and ramp control algorithms programmed as a VI on an FPGA module. User controls and indicators are programmed in an independent Host VI. An LVDT is employed as a position feedback sensor, while positioning accuracy and repeatability are experimentally assessed by using a laser interferometric system.

Numerous experiments with point-to-point positioning are conducted. In the first set of experiments short range positioning with 100 μm steps is validated. The calculated positioning accuracies and repeatabilities are always within 3 μm. Ramp control gives roughly two times better results than PID control.

In the case of long (10 mm) travel ranges, a marked nonlinearity is observed. It induces errors in the range of 40 – 50 μm. The nonlinear effect, caused mainly by the LVDT feedback sensor, is characterised via interferometric measurements and compensated via system linearization. The resulting linearizing analytical function is thus programmed in the LabVIEW Host VI. Positioning accuracy and repeatability are finally assessed experimentally again, and their values are limited to roughly 2 µm, both in the case of the PID and of the ramp control algorithms.

In a future work, the authors plan to investigate the usage of more complex control typologies, e.g. by implementing on the FPGA module a pulse-width modulation (PWM) based control. Means of optimising the control algorithms so as to maximise positioning accuracy and repeatability will also be investigated. Other types of feedback transducers, e.g. optical encoders, will be tested as well. Finally, multi-axes micropositioning mechatronics systems based on the described FPGA architecture will be developed. Their foreseen applications are in machine tools, devices for handling and assembly of microsystems, robotics, metrology, high-end optical system, scientific instrumentation, ICT, medicine and the growing micro-electro-mechanical (MEMS) devices field.

List of Symbols

A	power operational amplifier voltage gain [V/V]
b	ball bearing width [mm]
B	ball screw nominal maximum backlash [µm]
d	ball bearing inner diameter [mm]
d_0	ball screw nominal diameter [mm]
d_1, d_2	coupling inner diameters [mm]
D	ball bearing outer diameter [mm]
D_C	coupling nominal outer diameter [mm]
$e(k)$	value of integral error term in the discrete domain [mm]
$e(n)$	value of proportional and derivative error terms in the discrete domain [mm]
$e(t)$	error value [mm]
$f(x)$	LVDT linearization function [mm]
i	planetary gearhead reduction ratio
I_H	DC actuator stall current [mA]
$I_{\max}$	power operational amplifier maximum output current [A]
I_0	DC actuator no-load current [mA]
k	summation variable for the discrete integral term
K_P, K_I, K_D	proportional, integral and derivative controller gains of the PID controller
l	LVDT measurement range [mm]
l_C	coupling length [mm]
$l_f/w_f/h_f$	guideways' fixed part dimensions (length/width/height) [mm]
$l_m/w_m/h_m$	guideways' moving part dimensions (length/width/height) [mm]
L	DC motor length [mm]
L_g	planetary gearhead length [mm]
n	discrete time step
n_0	DC motor no load speed [rpm]
p	ball screw lead [mm]
r	theoretical LVDT resolution [µm]
t	time [s]
T	sampling period [s]
T_I, T_D	integral and derivative time constants [s]
$u(t)$, $u(n)$	output of the controller [V]
U_N	DC motor nominal voltage [V]
$V_{AO/I}$	FPGA module analog input/output full scale voltage [V]
$V_{BICM\max}$	BICM full scale range output DC voltage [V]
V_e	LVDT excitation voltage [V]
$V_{R\max}$	maximal voltage of ramp control algorithm [V]
$V_{R\min}$	minimal voltage of ramp control algorithm [V]
x	current LVDT position (displacement) [mm]
$y(t)$, $y(n)$	reached position (process value) [mm]
$y_0(t)$	reference position (set point) [mm]
η_p	ball screw practical efficiency [%]
τ	integration variable
ϕ	DC motor diameter [mm]

References

[1] S. Fukada, B. Fang and A. Shigeno, "Experimental analysis and simulation of nonlinear microscopic behaviour of ball screw mechanism for ultra precision positioning," Precision Engineering, vol. 35/3, pp. 650-668, 2011.

[2] K. H. Kim, P. J. Kim and K. H. You, "Ultra-precision positioning system using robust sliding mode observer and control," Precision Engineering, vol. 37/1, pp. 235-240, 2013.

[3] S. Zelenika and F. De Bona, "Nano-positioning using an adaptive pulse width approach," J. Mechanical Engineering Science – Proc. Institution Mech. Engineers, vol. 223/C8, pp. 1955-1963, 2009.

[4] B. A. Bucci, J. S. Vipperman, D. G. Cole and S. J. Ludwick, "Evaluation of a servo settling algorithm," Precision Engineering, vol. 37/1, pp. 10-22, 2013.

[5] E. Bin Linggin, "DC motor position control with PID controller," Fakulti Kejuruteraan Elektrik, Kolej Universiti Teknikal Kebangsaan Malaysia, 2005.

[6] URL: http://www.ni.com/fpga

[7] Y. P. Kondratenko and E. Gordienko, "Implementation of the neural networks for adaptive control system on FPGA," Annals of DAAAM & Proc. 23rd Int. DAAAM Symp., vol. 23, pp. 389-392, 2012.

[8] B. Mac Cleery and Z. M. Kassas, "New mechatronics development techniques for FPGA-based control and simulation of electromechanical systems," Proc. 17th World Congress – Int. Federation Automatic Control, Seoul, pp. 4434-4439, 2008.

[9] F. H. Ali, M. M. Hussein and S. M. B. Ismael, "LabVIEW FPGA implementation of a PID controller for DC motor speed control," Iraq J. Electrical and Electronic Engineering, vol. 2, pp. 139-144, 2010.

[10] URL: http://www.faulhaber.com/uploadpk/EN_1724_SR_DFF.pdf

[11] URL: http://www.omega.com/pptst/LD610.html

[12] URL: http://www.omega.com/manuals/manualpdf/M3342.pdf

[13] S. Fukada, M. Matsuyama and J. Hirayama, "Ultraprecision positioning with sub-nanometer resolution by using ball screw and aerostatic guide way," Proc. 12th Euspen Int. Conf., Stockholm, pp. 306-310, 2012.

[14] URL: http://www.skf.com/files/264744.pdf

[15] URL: http://www.skf.com/skf/productcatalogue/Forwarder?newlink=&action=search&lang=en&prodid=1010026184

[16] URL: http://in.misumi-ec.com/asia/ItemDetail/10300119820.html

[17] URL: http://www.schneeberger.com/products/linear-and-profiled-guideways/profiled-miniature-guideway/minirail-mini-x/#c2106

[18] URL: http://sine.ni.com/nips/cds/print/p/lang/hr/nid/201565

[19] URL: http://www.ni.com/pdf/products/us/20055052501101iLR.pdf

[20] URL: http://sine.ni.com/ds/app/doc/p/id/ds-98/lang/hr

[21] URL: http://www.ti.com/lit/ds/symlink/lm675.pdf

[22] URL: http://sine.ni.com/np/app/main/p/docid/nav-104/lang/hr

[23] URL: http://www.ni.com/pdf/manuals/373427c.pdf

[24] URL: http://lasertex.eu/pages,download.htm

[25] C. R. Steinmetz, "Sub-micron position measurement and control on precision machine tools with laser interferometry," Precision Engineering, vol. 12/1, pp. 12-24, 1990.

[26] G. F. Franklin, J. D. Powel and A. Emami-Naeini, "Feedback control of dynamic systems," Addison-Wesley series in electrical and computer engineering: control engineering, 2nd ed., 1991.

[27] URL: http://lorien.ncl.ac.uk/ming/digicont/digimath/dpid1.htm

[28] URL:http://www.palgrave.com/science/engineering/wilkie/sample/0333_77129Xcha18sample.pdf

[29] URL:http://www.ee.up.ac.za/main/_media/en/undergrad/subjects/ebt410/skogestad_simple_pid_tuning_rules.pdf

[30] URL: http://www.mathworks.com/help/signal/ref/interp.html